DEVELOPMENT AND EVALUATION OF STORM SURGE WARNING SYSTEM IN TAIWAN

MEI-YING LIN[1*], MING-DA CHIOU[2], CHIH-YING CHEN[3],
HAO-YUAN CHENG[4], WEN-CHEN LIU[5], and WEN-YIH SUN[6]
[1]Taiwan Typhoon and Flood Research Institute, National Applied Research Laboratories, Taiwan.
[2]Institute of Oceanography, National Taiwan University, Taiwan.
[3]Department of Land, Air and Water Resources, University of California, Davis, California, USA.
[4]Graduate Institute of Hydrological & Oceanic Sciences, National Central University, Taiwan.
[5]Department of Civil and Disaster Prevention Engineering, National United University, Taiwan
[6]Department of Earth, Atmospheric, and Planetary Sciences, Purdue University, USA.

ABSTRACT

We used three numerical experiments for developing and evaluating a storm surge warning to examine the performance of storm surge forecasting when triggered by typhoon forecasts from TAPEX (Taiwan Cooperative Precipitation Ensemble Forecast Experiment) and to identify the characteristics of storm surges along Taiwan's coast. The results show that the accuracy of storm surge forecasting is dominated by the track, the intensity, and the driving flow of a typhoon. However, in some cases, e.g., Typhoon Soulik in 2013, the wave effect on storm surges is not negligible, and the simulations exhibit a significant bias. To determine the source of this discrepancy, we observed surge deviations from the tide gauge measure for 23 typhoon events and found that the distribution of maximum surge heights peaks at both 40 and 160 cm. Since mechanisms for the rise in water level to 160 cm are not induced only by a storm forcing, we proposed that the wave effect on storm surges was responsible for the bias at this specific location. Due to the lack of observation of wave setup, this hypothesis was confirmed by results from the simulation of wind waves, which showed that an energetic wave pool lasted more than 6 hours along northeast Taiwan when Soulik passed. Wave breaking occurred when waves propagated to the coast and increased the water level there. Therefore, we suggest that the effect of wave breaking on storm surges should be considered for the next generation of storm surge warning systems along the northeastern coast of Taiwan.
Keywords: storm surge forecasting, ensemble forecast, uncertainty analysis

1 INTRODUCTION

According to Kinsman [1], storm surges can be categorized as forced waves since they propagate along with a typhoon. Scientists usually use shallow water equations to present the motion of storm surges; however, these simplifications become unrealistic when the typhoon moves near the shore. When a typhoon approaches landfall, the horizontal and vertical scales of surge motions are comparable, and the topography and the wave effect become significant. Resio & Westerink [2] pointed out that when modeling the physics of storm surges on the coast, local geometry, storm size, regional bathymetry, river discharge, and bottom drag play important roles and that any omission or simplification produces errors. However, including all mechanisms in a surge predicting system delays the warning process. Hence, when simplification is unavoidable, the sources of these resultant errors should be identified and classified.

Taiwan is located in a subtropical zone and experiences 3 to 4 typhoons annually, which cause the most common natural disasters on the island, including the potentially fatal catastrophe of heavy rainfall. The intensity of rainfall over the past 60 years has increased (Chang et al.[3]); the 12 heaviest rainfall events (exceeding 3500 mm within 48 hours), resulting from 8 typhoons, have occurred in the last 7 years. When rain falls on the land surface and forms floodwater, it runs quickly to the coast within 12 hours. The concentration time for mountainous topography is much shorter than for rivers. When excessive floodwater pours into the open ocean, the risk of inundation is low. However, when a storm surge blocks the gateway to the ocean, the risk of inundation increases, along with the depth and breadth of the affected area. One famous example is Typhoon Nari in 2010, which, due to heavy rainfall at the same time as storm surges and high tides, flooded the metro system in Taipei and left it inoperable for almost 6 months. Therefore, heavy rainfall and storm surges are two important factors for assessing the risk of inundation, and increased information about these factors will improve warning and mitigation strategies.

Regarding modeling and forecasting, the characteristics of a typhoon's rainfall pattern and its sensitivity to Taiwan's topography have been discussed in many studies [4]–[6]. Wang et al. [4] studied the influence of the Central Mountain Range (CMR) on rainfall and showed that an asymmetrical pattern forms on the lee side. Using ensemble simulations to analyze the uncertainty and predictability of rainfall from a typhoon influenced by CMR, Wu et al. [5] categorized patterns into three types associated with the northwesterly, westerly, and southwesterly tracks of a typhoon. Sun [6] also inferred that the interaction between a typhoon and the topography, including the important factor of surface friction (as interpreted by a detailed dynamical process), highly influences the shape, intensity, and track of the former. However, since the interaction is a highly nonlinear process, the uncertainty in rainfall forecasting is still difficult to eliminate. Lorenz [7] demonstrated that slightly differing initial states can evolve into considerably different states through nonlinear dynamical systems and that deterministic forecasting is unable to cover the uncertainties from initial. Therefore, some famous operational centers (Met Office; ECMWF, European Centre for Medium-Range Weather Forecasts; NCEP, National Centers for Environmental Prediction; and JMA, Japan Meteorological Agency) proposed an ensemble forecast that provides a confidence interval to cover the uncertainties and potential risks in numerical weather prediction (Bauer et al. [8]). This method has been applied to storm surge forecasts in many studies [9]–[13], including one typhoon event when typhoon and storm surge forecasts were unified to provide rainfall and storm surge information. In this study, we measure the performance of this approach by using TAPEX results as storm forcing and comparing our results with observation.

Previous studies ([14]–[17]) have indicated that storm surges are sensitive to typhoon forcing, tides, bottom topography, and wind waves, but ensemble typhoon forecasts do not account for these factors as of yet. Some observational and theoretical studies [18]–[20] have inferred that waves can increase the water level by 5–20% on a plain continental shelf and up to 35% on a steep bottom topography. Furthermore, numerical studies [21]–[24] also confirm that surge modeling improves when waves are included in the system. Sheng et al. [25] set up a test-bed for storm surges and coastal inundation models to examine whether using different grid systems or different numerical schemes affects the results; their findings indicate that no model appears to be consistently superior or inferior to any other. Therefore, the effect of numerical schemes on a surge modeling system will not be considered at this time, and we will instead focus on unresolved physical processes when significant errors occur in storm surge forecasting.

The organization of this paper is as follows: Section 2 describes the storm surge warning system and evaluates it according to three numerical experiments. Section 3 identifies the characteristics of storm surges at the Longdong station on the northeast coast of Taiwan in the past decade and notes that two peaks exist in the distribution of maximum surge heights. Wave setup may be another important mechanism that increases the water level at the Longdong station. Finally, Section 4 reports our main conclusions.

2 STORM SURGE WARNING SYSTEM AND EVALUATION

We evaluate the performance of the storm surge warning system (Fig. 1) and identify the characteristics of storm surges along Taiwan's coast by implementing three numerical experiments. The first experiment (NE I) establishes the framework of the system; the storm forcing is obtained from the WRF (Weather and Research Forecasting) Model members in TAPEX. The second experiment (NE II) uses a higher grid resolution and an advanced typhoon initialization scheme (Nguyen & Chen [26]) (NC scheme) to provide better prediction for typhoon movement. This experiment checks whether improved prediction of storm forcing also improves the prediction of storm surges. The storm forcing for the third experiment (NE III) is obtained from an analytic hurricane wind model in which the best track observation is included but the horizontal distribution of wind and pressure fields is idealized. The Holland wind model, which is widely used in engineering applications, is used as a basis of comparison.

2.1 Numerical experiments and modeling system

The framework for NE I is based on a joint typhoon and storm surge forecasting system that was developed using results from WRF Model members in TAPEX and POM (The Princeton Ocean Model). In terms of performance, TAPEX is comparable to ECMWF, NCEP, and JMA. The three-nested grid system is used by these typhoon forecasting members, and the grid resolution from the outer domain to the inner domain is 45, 15, and 5 kilometers, respectively. For the storm surge modeling system in NE I, the grid resolution is 15 kilometers, which is the same as the second nested domain in typhoon forecasting. A global tidal model (PXO6.2: TOPEX/POSEIDON), which is included in the surge modeling system, simulates the water level with tides and storm surges.

NE II implements the NC scheme, which is generated by a dynamical initialization method proposed by Nguyen & Chen [26] and offers a more realistic balance between the background circulation and the typhoon vortex. Chen et al. [27] provided a systematic evaluation of this method using 18 typhoon events and showed that the accuracy of the intensity forecast is improved. The margins of error for low central pressure and maximum wind can be smaller than 10 hPa and 10 m/s, respectively. The grid resolution of the three-nested domain for the typhoon model is 18, 6, and 2 km, and the resolution of the adjusted grid system for the surge model ranges from 1 to 15 kilometers.

For NE III, typhoon forcing is set up using the Holland wind model (Holland, [28]) and best track observational data. The grid resolution for both the typhoon and surge modeling systems is 15 km. This numerical experiment provides a baseline for comparison and shows the difference between analytic and real wind models for surge modeling results.

2.2 Performance of the storm surge warning system

Four typhoon events (Morakot in 2009, Fanapi in 2010, Saola in 2012, and Soulik in 2013) are used to evaluate the storm surge warning system; their tracks are shown in Fig. 2. We simulate the movements of these typhoons via the three methods described in numerical experiments I, II, and III. These storm forcings trigger storm surges, which are evaluated by tide gauge observation along Taiwan's coast (the stations are shown in Fig. 3).

2.2.1 Evaluation of storm forcing

Figs. 4–8 display the evaluation of storm forcing for NE I while 9 and 10 exhibit the comparison between NE I and NE II, revealing several issues.

The first issue concerns track errors, as the landfall location of a typhoon is an important factor in determining which watershed should be monitored. The suspected region for storm surge disasters is located on the path of a typhoon and within the maximum storm wind radius. Since the storm forcing from TAPEX is a type of ensemble forecast, ensemble spread is usually used to determine the range of forecasting errors (Barker, [29]; Grimit & Mass, [30]). Cases with large (or small) ensemble spread should be associated with large (or small) forecast uncertainty. Fig. 4 shows the track forecasts from TAPEX for Typhoons Saola in 2012 and Soulik in 2013, which indicate that forecasting from TAPEX can identify the trend of a typhoon; however, the ensemble spread for Saola is larger than that of Soulik. Since Soulik is a strong typhoon, whose path is less affected by Taiwan topography, its forecast uncertainty is small. The low central pressure is about 960 hPa for Saola (Fig. 5) and about 940 hPa for Soulik (Fig. 6). Hence, we expect that Soulik's simulation provides better forecasts, as shown in Section 2.3.

The second issue involves typhoon intensity forecasts, as the strength of storm surges is an important factor in determining the resistance to flood water at a river mouth. Since a storm surge is induced by the wind and pressure stresses of a typhoon, uncertainty in intensity forecasts decreases the reliability of storm surge forecasts. Therefore, we must determine which forecast run provides a more accurate intensity forecast. For example, Fig. 5 displays the results for central pressure from two runs on July 31 and August 1 for Saola. The lead time for landfall is approximately 48 and 24 hours for the former and latter runs, and the maximum difference among forecasting members for the lowest pressure is about 25 and 20 hPa, respectively. The later run provides a higher reliability. However, when the forecast is initiated very close to the time of landfall, it underestimates the intensity due to the influence of Taiwan's topography. As an example, Fig. 6 reveals that the central pressure for the run initiated on July 12 is higher than observation. Therefore, we evaluate a storm surge using forecast runs between 24 and 48 hours prior to landfall.

The third issue relates to the translation speed of a typhoon, as the timing of the storm surge is an important factor in determining river flooding. Fig. 7 exhibits three runs from NE I for Saola initiated at 18 UTC on July 31, 2012 (2012073118), 0 UTC on August 1, 2012 (2012080100), and 6 UTC on August 1, 2012 (2012080106), respectively. The uppermost panel shows a significant time lag for the storm surge forecast, indicating that the driving flow in the case of the 2012073118 run is slower than the other two. Hence, longer forecasts have more uncertainty in predicting the translation speed of a typhoon. Fig. 8 shows more results from different tide gauge stations (Longdong, Fulong, and Suao) near the location of landfall and more initiated runs (with lead times of 32, 26, 20, and 14 hours) for Saola. The dotted symbols represent results from different forecasting members, revealing a significant time lag for the runs with longer lead times.

A comparison of storm forcing between NE I and NE II is shown in Figs. 9 and 10. The track obtained from NE II (the blue dotted line) is almost consistent with observation (the black dotted line) (Fig. 9), and results for low central pressure (Fig. 10) are accurate. Since the main difference in storm forcing for NE II and NE III is the horizontal distribution of wind and pressure fields, we use this factor to assess whether the Holland wind model is applicable to the wind and pressure field around Taiwan.

2.2.2 Evaluation for storm surges

The level of seawater increases and propagates with a storm during storm surges, interacting with tides, wind waves, local geometry, and river flows. This phenomenon can be observed by tide gauge measurements with a sampling rate of every few minutes. However, our storm surge warning system does not consider the nonlinear interaction with wind waves or ocean currents. Thus, when we compare simulations of storm surges with observational data, we should anticipate some discrepancy. In this section, we identify sources of potential bias, as shown in Figs. 11–15.

Figs. 11 and 12 display the comparisons between observations and the three numerical experiments at different tide gauge stations. Tidal residual components from observation are obtained from the tool T_TIDE (Pawlowicz, [31]) in MATLAB. For Saola (Fig. 11), surges induced by NE I (the yellow lines) indicate a time lag compared to observation (the blue dotted line), but the surge induced by NE II (the red line) matches the timing of the latter. Since the timing for NE II and NE III (the green line) is consistent, we infer that the transmission speeds of a typhoon from simulation and observation are comparable, i.e., the method of simulation in NE II provides a better driving flow (background circulation) than in NE I.

The surge simulated by the Holland wind model incorporating observational data (NE III) is intended to minimize the bias in track between simulation and observation. However, results show that the bias along the east coast (at Longdong, Fulong, Suao, and Hualien) is smaller than along the west coast (at Danshuei and Kaohsiung), which suggests that the Holland wind model is insufficient for interpreting the horizontal distribution of wind and pressure fields for Saola. However, if a typhoon is strong enough (refer to the example of Soulik in Fig. 12), the results for stations along the west coast improve, which may be due to the typhoon's path being less affected by mountains.

Based on the timing and the intensity observed at the tide gauge stations, the simulated water levels for Soulik are generally more accurate than for Saola. However, Fig. 12 reveals significant underestimates for the former at Longdong and Fulong in northeastern Taiwan. Furthermore, this bias does not appear for Suao, a nearby station (as shown in Fig. 3) that experienced similar effects, which suggests that mechanisms other than errors from storm forcing must be responsible. Fig. 13, which compares simulations with observations of the surges for Morakot, Fanapi, Saola, and Soulik at Longdong and Suao, indicates that while the intensity of surges can be accurately predicted at Suao for these four typhoons, the intensity is underestimated at Longdong for Morakot and Soulik. Moreover, when we compare the timing (Fig. 14) and intensity (Fig. 15) of these typhoons with the results from NE I (black diamonds), NE II (red squares), and NE III (blue circles) at all stations, we discover that the simulations cannot predict the water level (as observed) at some locations (marked by arrows in Fig. 5). Fig. 16 shows the simulation of storm tides from NE II. Since the difference still exists, tide-surge interaction may not be responsible for the discrepancy between simulation and observation. In the next section, we examine clues that suggest this bias may be produced by the effect of wind waves.

3 OBSERVATIONS AND ANALYSIS

The discrepancy between forecasts and observation indicates that the storm surge warning system failed to provide accurate forecasts about Soulik and Morakot along the northeast coast of Taiwan (at Longdong and Fulong). As exhibited in Fig. 13, Soulik caused a far higher increase in water level at Longdong than Saola, but the increase in water level at Suao was approximately the same for both typhoons. Since the distance between Suao and Longdong is only about 50 kilometers, we conjecture that waves may account for the difference. Due to the lack of observational data on wave height, we simulated wind waves and the distribution of surge height from historical typhoon events as references.

Fig. 17 displays the observational data for storm surges in the past 11 years. The red and blue lines represent the tide gauge observation and the tidal residual component, respectively. Each rise in water level (the blue line) is related to a typhoon event, and it is evident that the storm surges induced by Talim in 2005, Krosa in 2007, Jangmi in 2008, Morakot in 2009, and Soulik in 2013 are much larger than other events. These typhoons followed a similar track as Soulik, over northeastern Taiwan. Fig. 18 exhibits the distribution of surge height for these 23 events and reveals two peaks (40 and 160 cm). Thus, it can be inferred that the mechanism differs for these two groups. In the first group, the range of surge falls between 20 and 120 cm, with the peak located at 40 cm, while in the second, the range of surge deviation falls between 160 and 180 cm. Hence, as evident in Fig. 19, the water level at Longdong does not depend only on storm intensity.

The relation between the pressure gradient and the surge deviation is about 0.56 (upper panel), and the relation between the wind gradient and the surge deviation (lower panel) is about 0.18, indicating that the rise in water level is due more to the inverse barometer effect than wind setup. However, since the inverse barometer effect would not solely cause the water level to rise to this extent (160 cm), we assume that wave setup is also responsible. Figs. 20 and 21 exhibit the distribution of wind waves when Saola and Soulik passed over the northeast coast of Taiwan. Although Longdong is located on the windward side of these two events, the significant wave height for Soulik (about 15 m) is much larger than for Saola (less than 10 m), which implies that an extremely large amount of wave energy dissipated on the coast and produced the rise in water level. This energy pool lasted for approximately 6 hours, indicating that the rise in water level due to wave setup existed for the same span of time as the rise due to storm forcing. According to experimental results for wave setup (Holman & Sallenger [32]), the level can reach 72 cm when the wave height is 15 m for a bottom slope of 0.02 and a wave period of 15 s. Since the amount of wave setup obtained from this empirical formula is consistent with the discrepancy between the simulation from NE II and observation, we suggest that the bias at Longdong is due to surface waves.

3 CONCLUSIONS

The ensemble forecast of a typhoon usually provides warning information for atmospheric-related factors, such as the track, intensity, and rainfall amount, but it tends to be less concerned with flooding due to river-blocking storm surges, the timing of which depends on the driving force. Therefore, forecasts for both storm surges and rainfall must be combined in order to accurately identify areas that will be inundated during a typhoon, allowing risk managers to implement effective measures for disaster mitigation.

Our numerical experiments evaluated the performance of a storm surge warning system based on a joint forecast for typhoon and surges. The first experiment (NE I) examined the operational warning system. 12 forecasting members provided warning information for storm surges, and, prioritizing efficiency, the grid resolution of the modeling system was set to 15 km. The second experiment (NE II) provided a more accurate prediction based on a higher grid resolution and an advanced typhoon initialization scheme, but it required far more computing time than NE I. The finest grid resolution for storm surge was set to 1 km on the northeast coast of Taiwan, where Saola and Soulik made landfall. The third experiment (NE III) employed an analytic wind model using the best track data to mimic the movement of a typhoon. Since this idealized model cannot address Taiwan's topography, the horizontal wind structure is not as realistic as NE I and NE II.

The results from these experiments indicate that storm surges are dominated by storm forcing and then influenced by their interactions with wind waves, local geometry, and tides. The track, intensity, and transmission speed of a typhoon determine the location, strength, and timing of surges. When a typhoon passes over northeastern Taiwan, wave effect also becomes significant.

ACKNOWLEDGEMENTS

This research was partly supported by projects from the Institute of Nuclear Energy Research (NL102124 & NL1031373). Computational resources were provided by the National Center for High-Performance Computing. Tide gauge observations were provided by the Central Weather Bureau. We thank Ming-Hwi Sun for English editing.

REFERENCES

[1] Kinsman, B., *Wind waves: their generation and propagation on the ocean surface*, Prentice-Hall Inc., Englewood Cliffs, New Jersey, 676pp, 1956.

[2] Resio, D. T. & Westerink J. J., Modeling the physics of storm surges, *Physics Today*, Vol. **61, No.** 9, pp.33-38, 2008.

[3] Chang, et al., Large increasing trend of tropical cyclone rainfall in Taiwan and the roles of terrain, *J. Climate*, Vol. **26**, pp.4138-4147, 2013.

[4] Wang, et al., Sensitivity of typhoon track to asymmetric latent heating/rainfall induced by Taiwan topography: A numerical study of typhoon Fanapi (2010), *J. Geophys. Res.: Atmos*., Vol. **118**, pp.3292-3308, 2013.

[5] Wu, et al., Uncertainty and predictability of tropical cyclone rainfall based on ensemble simulations of typhoon Sinlaku (2008), *Mon. Wea. Rev.*, Vol. **141**, pp.3517-3538, 2013.

[6] Sun, W.-Y., The vortex moving toward Taiwan and the influence of the central mountain range, *Geosci. Lett.*, Vol. **3,** No. 21, pp.1-19, 2016.

[7] Lorenz, E.N., Predictability: does the flap of a butterfly's wings in Brazil set off a tornado in Texas?, *139th Annual Meeting of the American Association for the Advancement of Science*, 1972.

[8] Bauer, et al., The quiet revolution of numerical weather prediction, Nature, Vol. **25**, pp.47-55, 2015.

[9] Flowerdew, et al., Development and evaluation of an ensemble forecasting system for coastal storm surges, *Q. J. R. Meteorol. Soc.*, Vol. **136**, pp.1444-1456, 2010.

[10] DI Liberto, et al., Verification of a multimodel storm surge ensemble around New York City and Long Island for the cool season, *Weather and Forecasting*, Vol. **26**, pp. 922-939, 2011.

[11] Flowerdew, et al., Extending the forecasting range of the UK storm surge ensemble, *Q. J. R. Meteorol. Soc*., Vol. **139**, pp.184-197, 2013.

[12] Flowerdew J, Horsburgh K, Wilson C, Mylne K. 2010. Development and evaluation of an ensemble forecasting system for coastal storm surges. *Q. J. R. Meteorol. Soc.* **136**: 1444–1456.

[13] Condon, et al., Toward high-resolution, rapid, probabilistic forecasting of the inundation threat from landfalling hurricanes, *Mon. Wea. Rev.*, Vol. **141**, pp.1304-1323, 2012.

[14] Suh et al., An efficient early warning system for typhoon storm surge based on time-varying advisories by coupled ADCIRC and SWAN, *Coean Dynamics*, Vol. **65**, pp. 617-646, 2015.

[15] Sheng et al., Simulating storm surge and inundation along the Taiwan Coast during typhoons Fanapi and Soulik in 2013, *Terr. Atmos. Coean. Sci.*, Vol. **27**, No. 6, pp. 1-15, 2016.

[16] Chiou, M.-D., Characteristic and numerical simulation of astronomic tide and storm surge in Taiwan water, National Cheng Kung University, Ph.D. thesis, 157pp, 2010.

[17] Liou, J. M. & Chen, S. H., Effect of the wave set-up on the estimation of storm surge in the coastal waters, *Taiwan Water Conservancy*, Vol. **63**, pp. 83-92, 2015.

[18] Chen, W.-B. & Liu, W.-C., Assessment of storm surge inundation and potential hazard

maps for the southern coast of Taiwan, Natural Hazards, Vol. 82, pp. 591-616, 2016.
[19] Longuet-Higgins, M. S. & Stewart, R. W., Radiation stress in water waves; a physical discussion, with applications, *Deep-Sea Res.*, Vol. 11, pp.529-562, 1964.
[20] Kim, et al., Wave set-up in the storm surge along open coasts during Typhoon Anita, *Coastal Engineering*, Vol. **57**, pp.631-642, 2010.
[21] Hsu, et al., Wave setup and setdown generated by obliquely incident waves, *Coastal Engineering*, Vol. **53**, pp. 865-877, 2006.
[22] Bunya, et al., A high-resolution coupled riverine flow, tide, wind, wind wave, and storm surge model for Southern Louisiana and Mississippi. Part I: Model development and validation, *Mon. Wea. Rev.*, Vol. **138**, pp. 345-377, 2010.
[23] Funakoshi, Y., Coupling of hydrodynamic and wave models for storm tide simulations: A case study for hurricane Floyd (1999), Ph. D. thesis, 235pp, 2006.
[24] Dietrich, et al., Modeling hurricane waves and storm surge using integrally-coupled, scalable computations, *Coastal Engineering*, Vol. **58**, pp. 45-65, 2011.
[25] Sheng, et al., A regional testbed for storm surge and coastal inundation models-An Overview, *Estuarine and Coastal Modeling*, pp.476-495, 2012.
[26] Nguyen, H.V., & Chen, Y.-L., Improvements to a Tropical Cyclone Initialization Scheme and Impacts on Forecasts, *Mon. Wea. Rev*., Vol. **142**, pp.4340-4356, 2014.
[27] Chen, et al., The spin-up processes of a cyclone vortex in a tropical cyclone initialization scheme and its impact on the initial TC structure, *SOLA*, Vol. **10**, pp.93-97, 2014.
[28] Holland, G. J., An analytic model of the wind and pressure profiles in hurricanes, *Mon. Wea. Rev*., Vol. **108**, pp. 1212–1218, 1980.
[29] Grimit, E. P. & Mass, C. F., Measuring the ensemble spread-error relationship with a probabilistic approach: Stochastic ensemble results, Mon. Wea. Rev., Vol. 135, pp. 203-221, 2007.
[30] Barker, T. W., 1991, The relationship between spread and forecast error in extended-range forecasts. J. Climate, 4, 733-742.
[31] Holman, R. A., & Sallenger, A. H., Set-up and swash on a natural beach, *J. Geophys. Res.* Vol. **90**, pp. 945–953, 1985.
[32] Pawlowicz, et al., Classical tidal harmonic analysis including error estimates in MATLAB using T_TIDE, *Computers and Geosciences*, Vol. 28, pp.929-937, 2002.

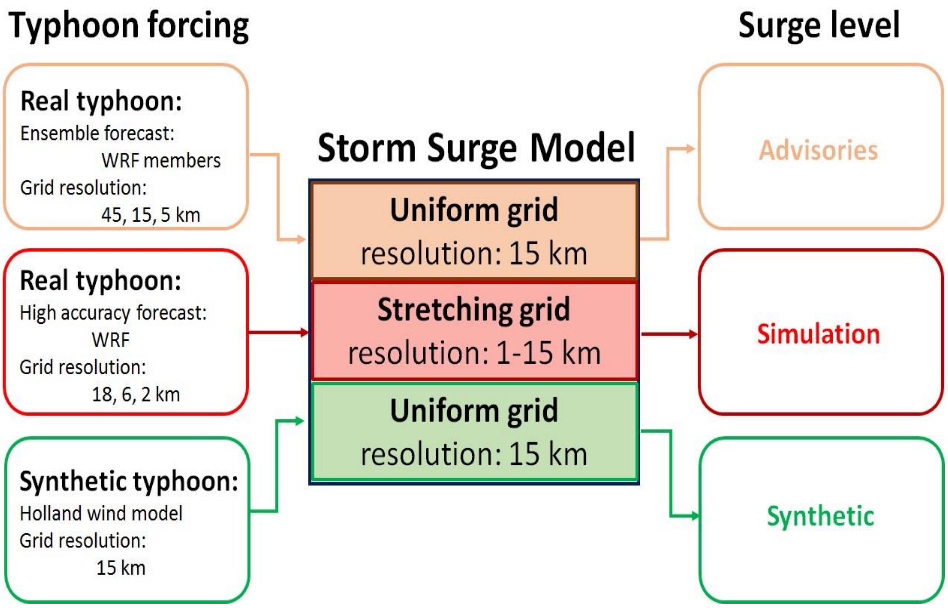

Figure 1: Three numerical experiments for the evaluation of a storm surge warning system with different typhoon forcings and grid resolutions.

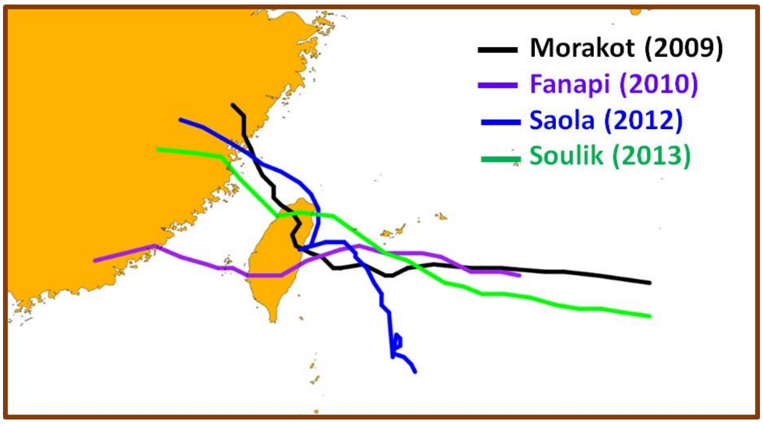

Figure 2: The tracks of Morakot, Fanapi, Saola, and Soulik.

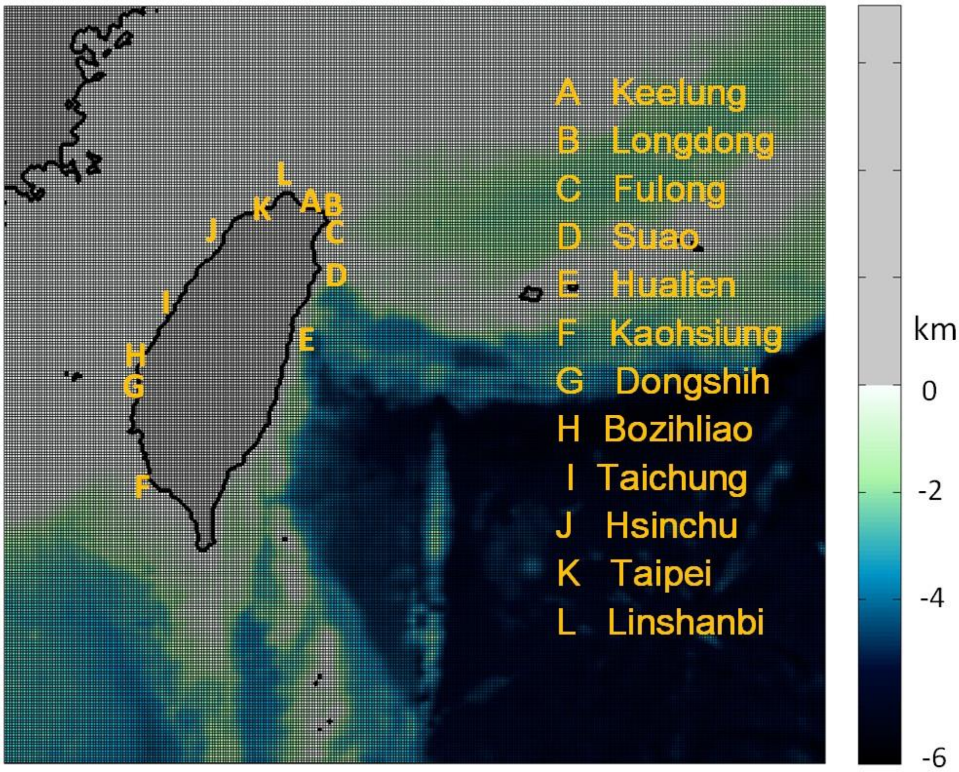

Figure 3: The locations of twelve tide gauge stations.

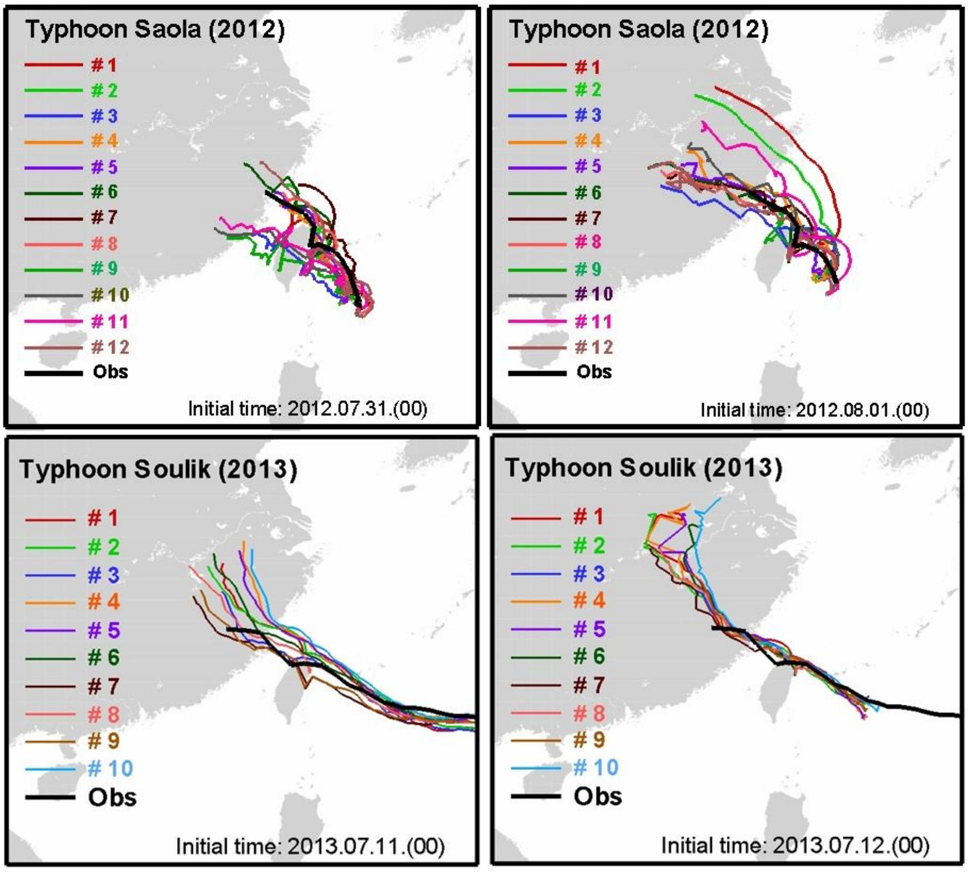

Figure 4: Track forecasts for Saola in 2012 (upper two panels) and Soulik in 2013 (lower two panels) at two initials juxtaposed with observed tracks.

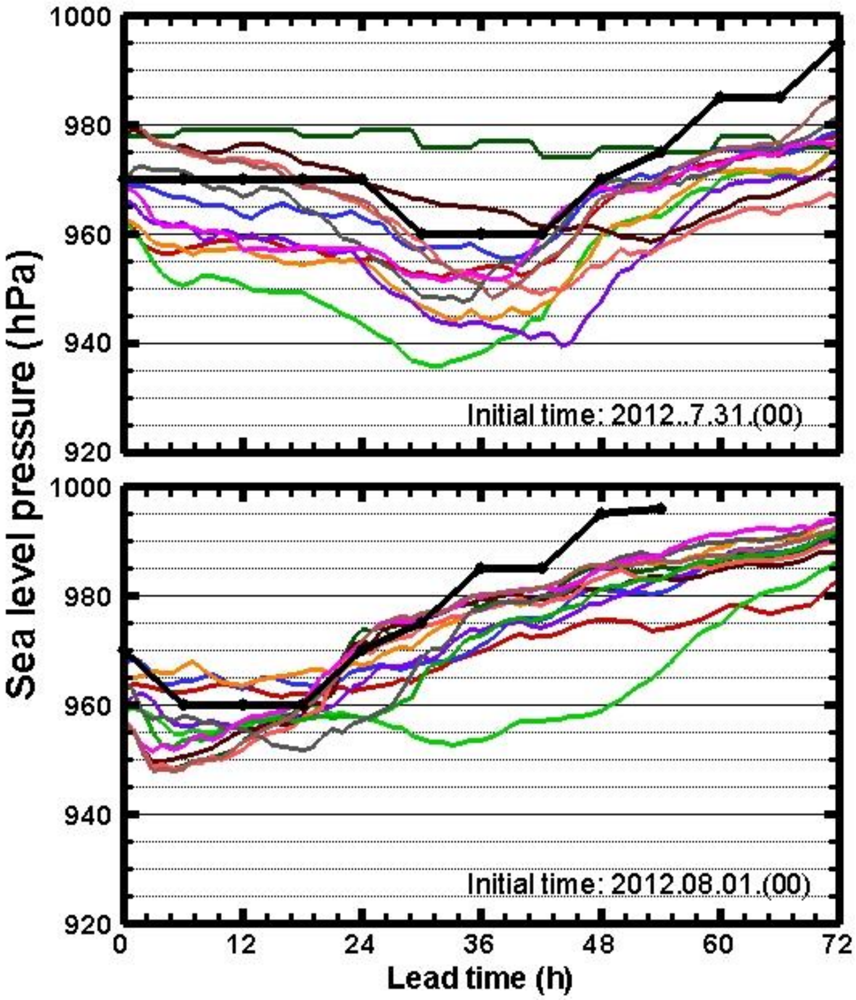

Figure 5: Central pressure forecasts for Saola at two initials juxtaposed with observed pressure. Line legend is identical to Fig. 4.

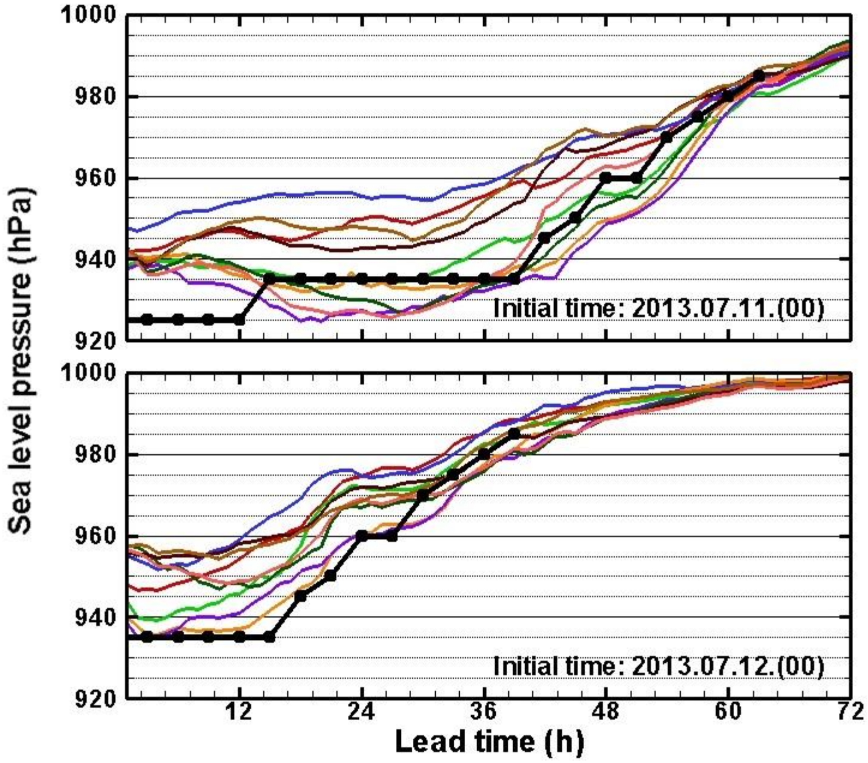

Figure 6: Central pressure forecasts for Soulik at two initials juxtaposed with observed pressure. Line legend is identical to Fig. 4.

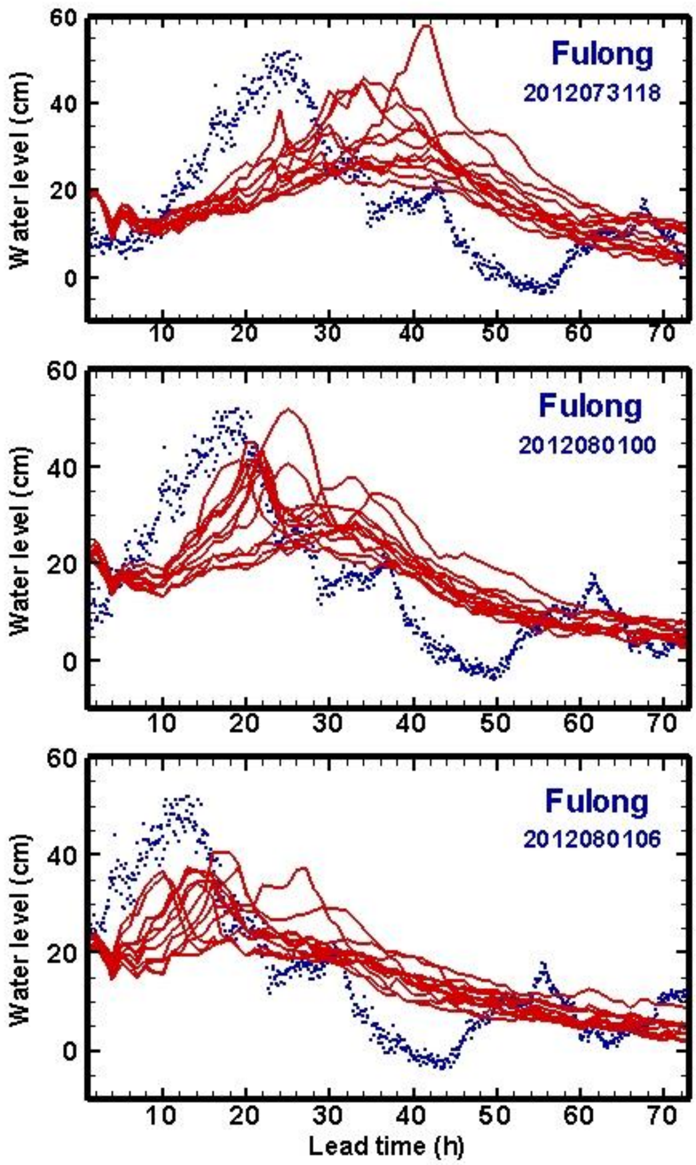

Figure 7: Observations (blue dot) and NE I simulations (red line) of Saola at three initials at Flong station.

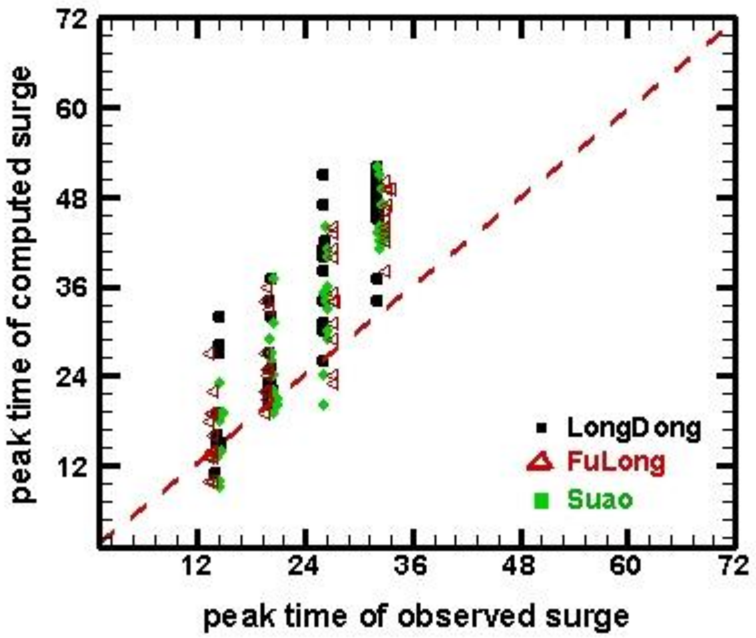

Figure 8: Peak times of observed and computed surges at Longdong, Fulong, and Suao stations for four initials.

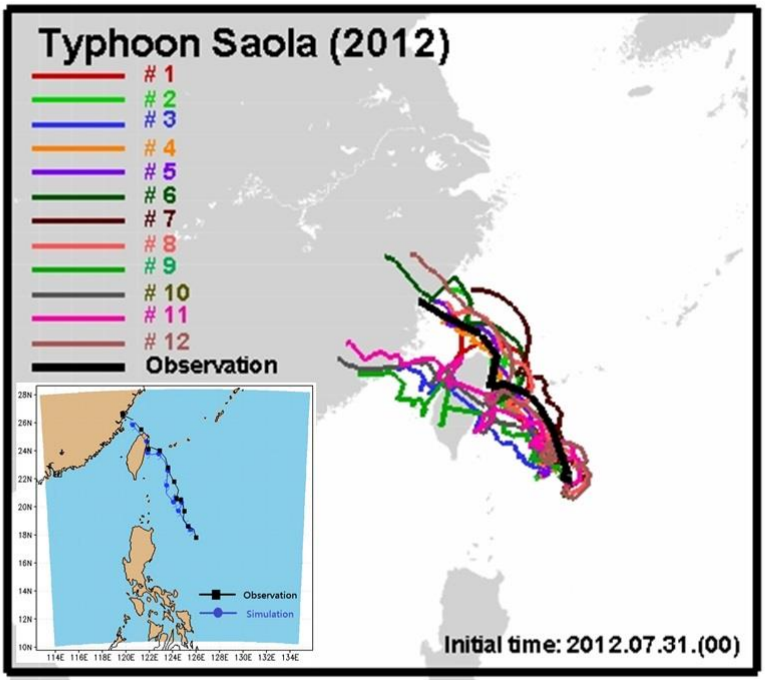

Figure 9: Track forecasts from NE I (colored lines) and NE II (blue dotted line) juxtaposed with observed track (black or black dotted lines) for Saola.

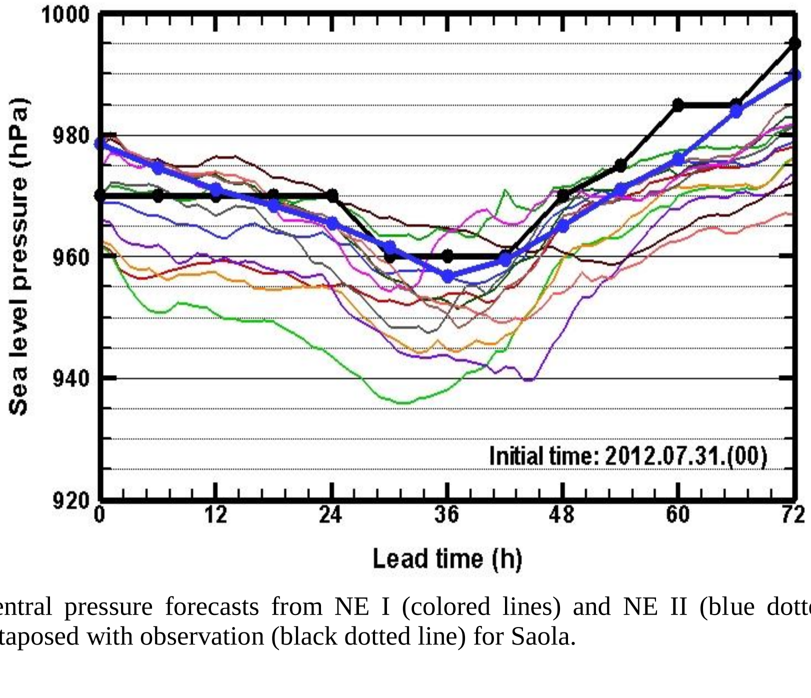

Figure 10: Central pressure forecasts from NE I (colored lines) and NE II (blue dotted line) juxtaposed with observation (black dotted line) for Saola.

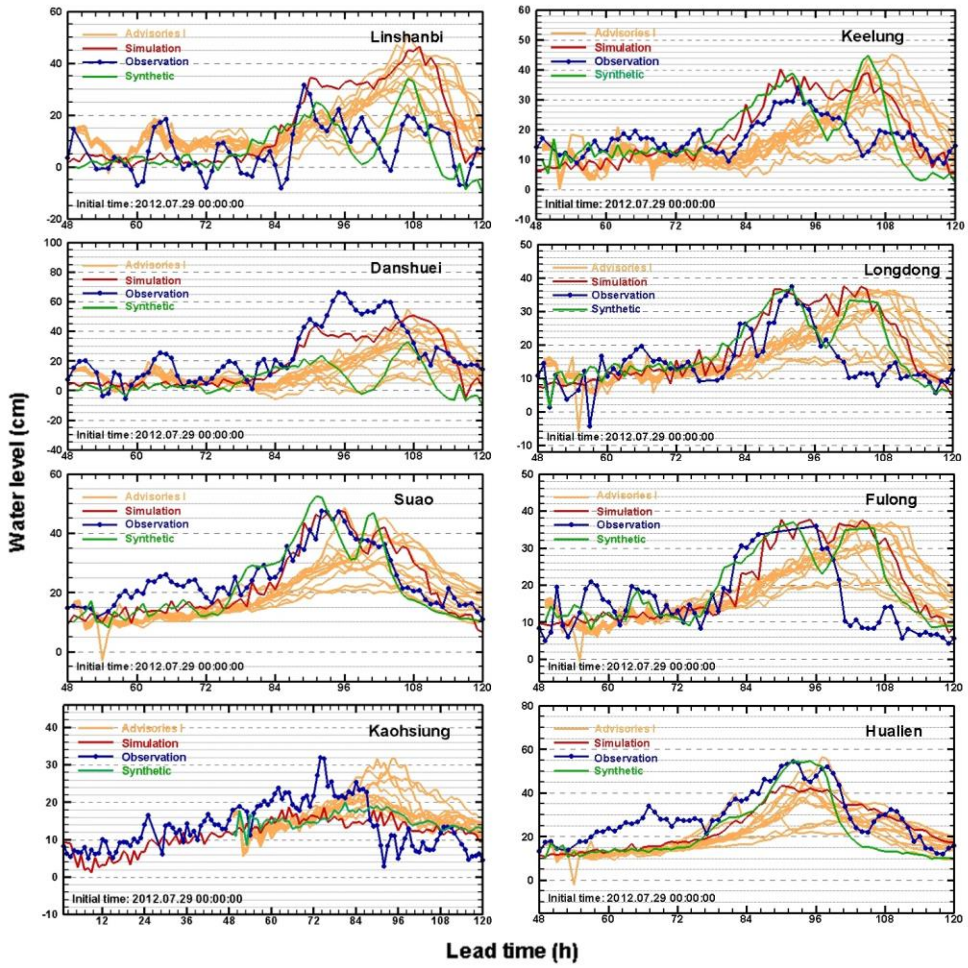

Figure 11: Simulations of surges for Saola in 2012 from NE I (yellow lines), NE II (red line), and NE III (green line) juxtaposed with observation (blue dotted line) at eight tide gauge stations.

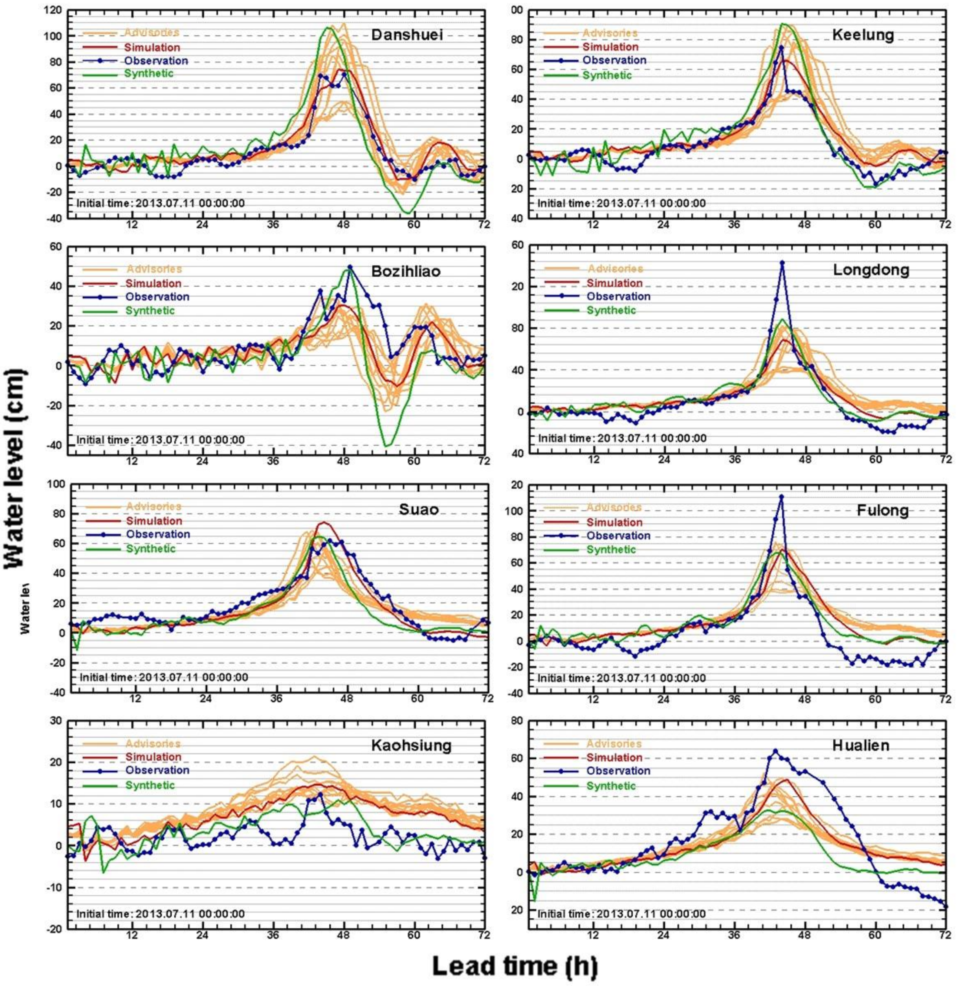

Figure 12: Simulations of surges for Soulik in 2012 from NE I (yellow lines), NE II (red line), and NE III (green line) juxtaposed with observation (blue dotted line) at eight tide gauge stations.

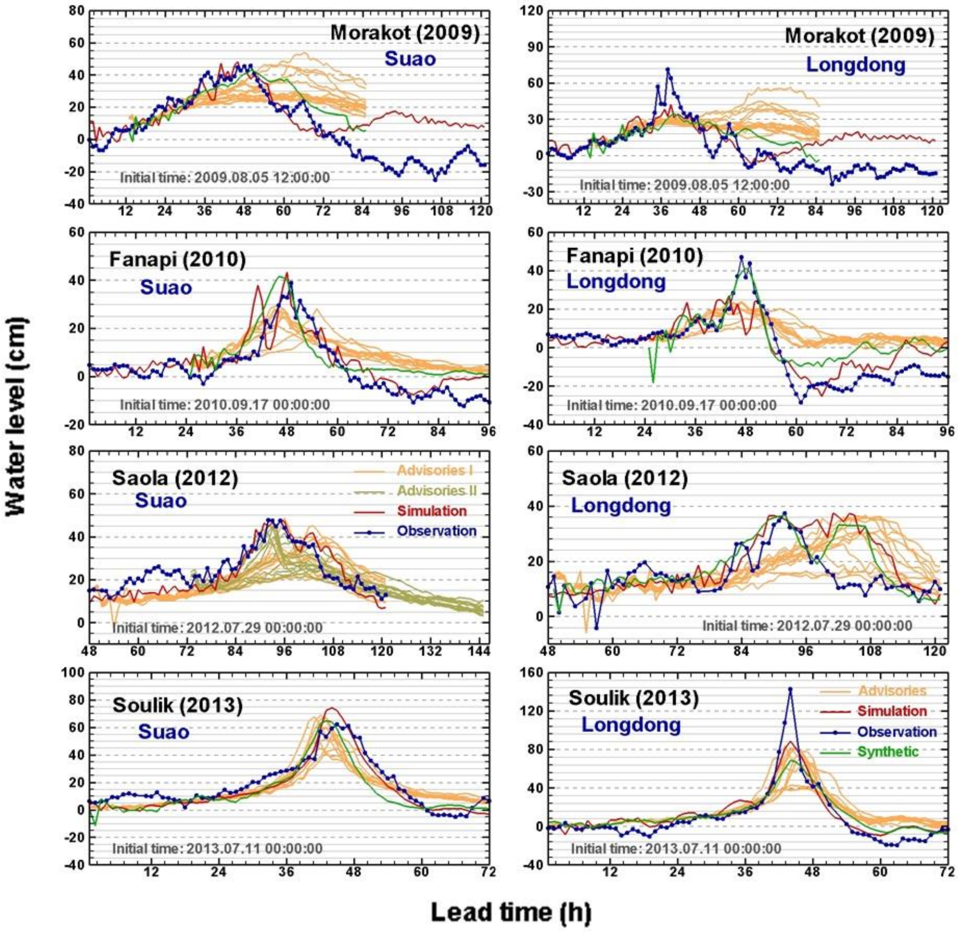

Figure 13: Simulated and observed surges for Morakot, Fanapi, Saola, and Soulik (from top to bottom panels) at Suao (left panels) and Longdong (right panels) tide gauge stations.

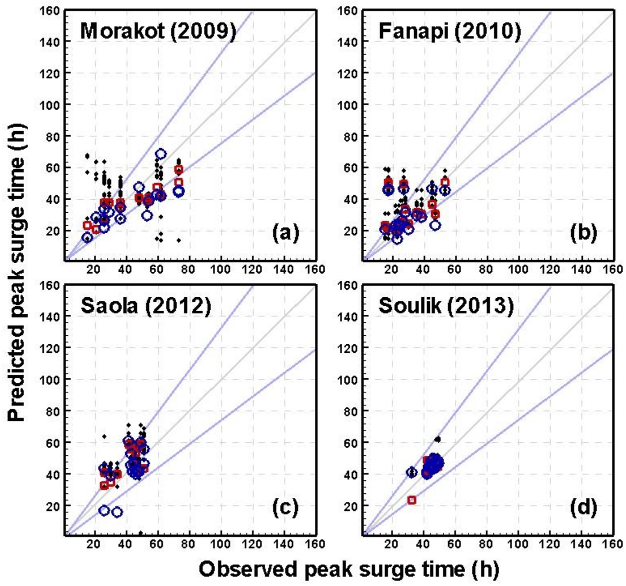

Figure 14: Predicted and observed peak surge time for Morakot, Fanapi, Soala, and Soulik. Blue symbols: NE III; red symbols: NEII; black symbols: NE I.

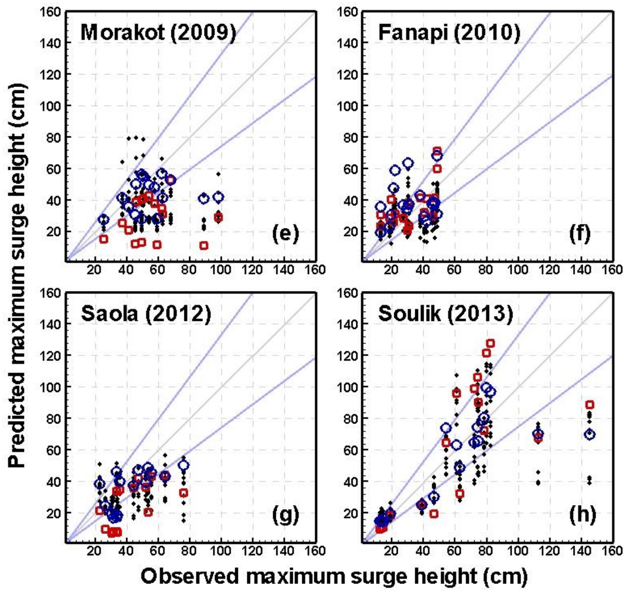

Figure 15: Predicted and observed maximum surge height for Morakot, Fanapi, Soala, and Soulik. Blue symbols: NE III; red symbols: NEII; black symbols: NE I.

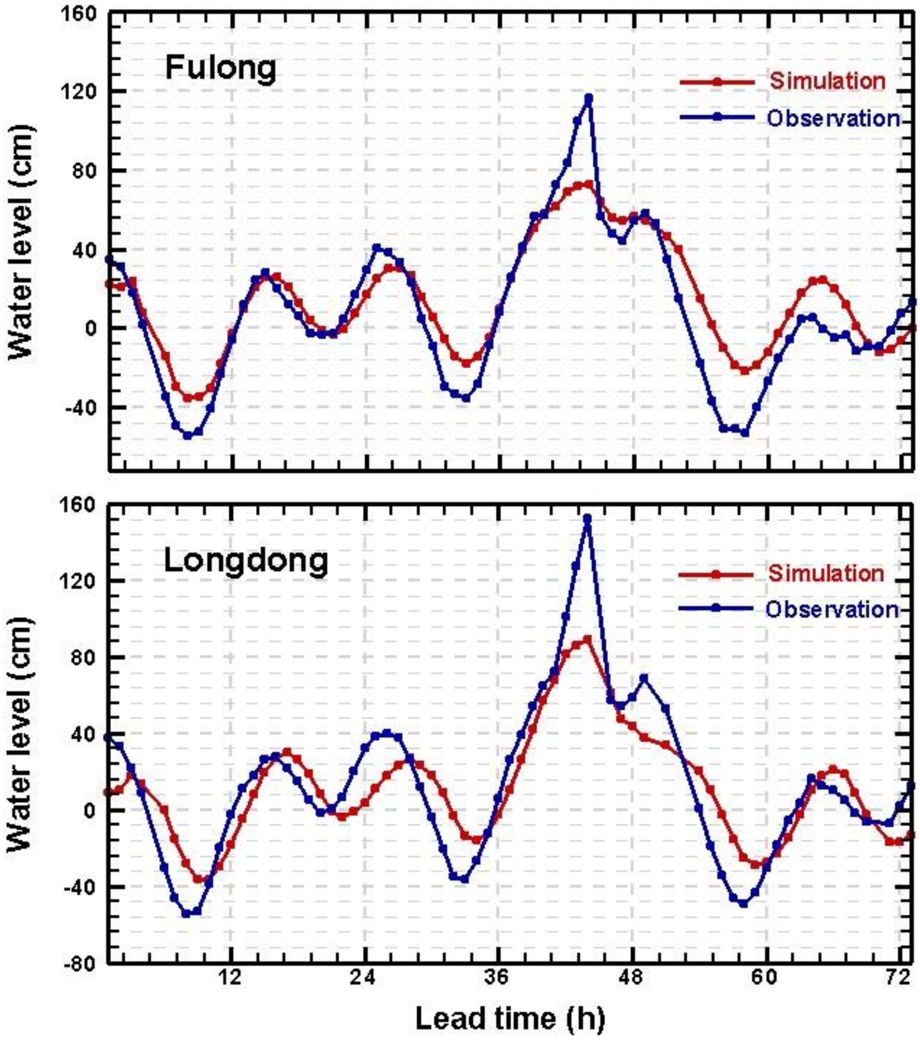

Figure 16: Simulated storm tides from NE II (red dotted line) juxtaposed with observed tides (blue dotted line) for Soulik at Fulong (upper panel) and Longdong (lower panel) tide gauge stations.

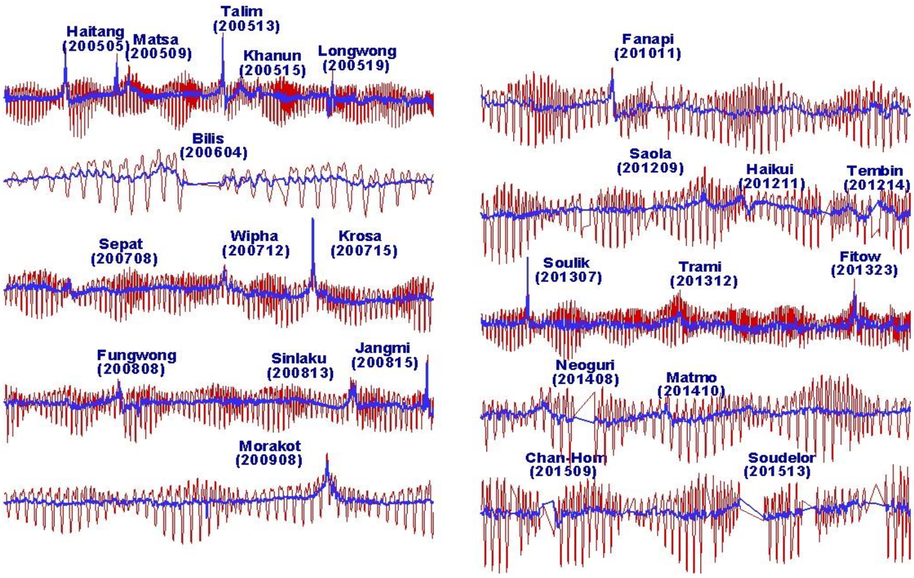

Figure 17: Eleven years (2005–2015) of tide gauge observation (red line) and tidal residuals (blue line) at Longdong station.

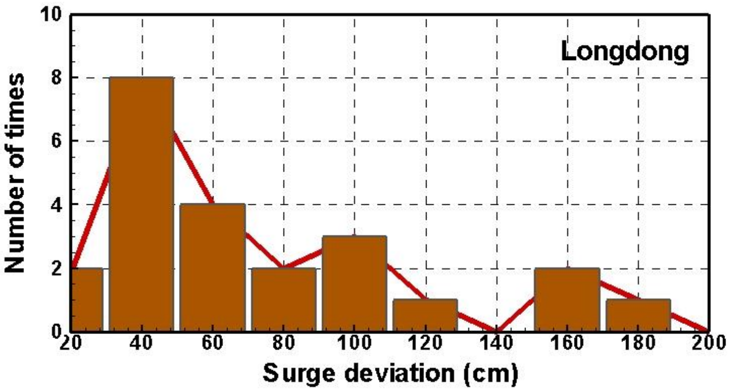

Figure 18: Surge density distribution for 23 typhoon events from 2005 till 2015 at Longdong station.

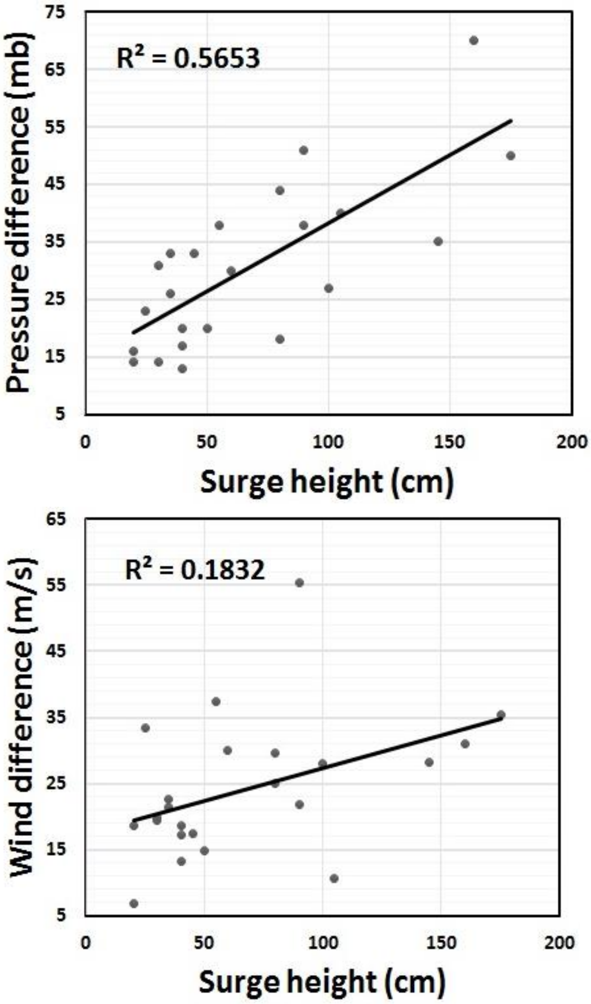

Figure 19: Correlation coefficients for surge height and pressure gradient (upper panel) and for surge height and wind gradient (lower panel).

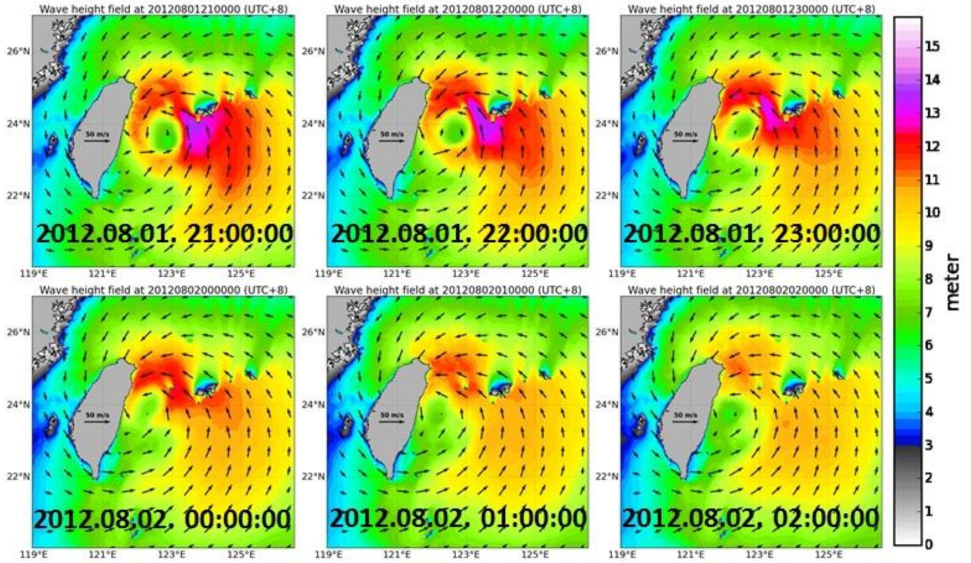

Figure 20: The distribution of simulated significant wave height (color) and wind (arrow) for Saola.

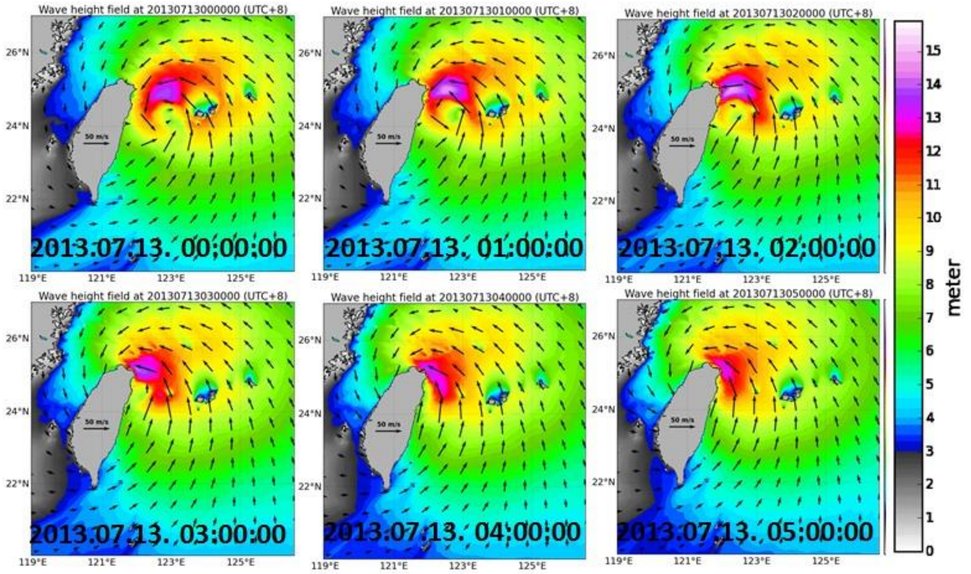

Figure 21: The distribution of simulated significant wave height (color) and wind (arrow) for Soulik.